

GENERATION OF MAGNETIC FIELD ON THE ACCRETION DISK AROUND A PROTO-FIRST-STAR

YUKI SHIROMOTO, HAJIME SUSA

Department of Physics, Konan University, Kobe 658-8501, Japan¹

TAKASHI HOSOKAWA

Department of Physics and Research Center for the Early Universe, The University of Tokyo, Tokyo 113-0033, Japan²

Draft version March 15, 2022

ABSTRACT

The generation process of magnetic field around a proto-first-star is studied. Utilizing the recent numerical result of proto-first-star formation based upon the radiation hydrodynamics simulations, we assess the magnetic field strength generated by the radiative force and the Biermann battery effect.

We find that magnetic field of $\sim 10^{-9}$ G is generated on the surface of the accretion disk around the proto-first-star. The field strength on the accretion disk is smaller by two orders of magnitude than the critical value, above which the gravitational fragmentation of the disk is suppressed. Thus, the generated seed magnetic field hardly affect the dynamics of on-site first star formation directly, unless efficient amplification process is taken into consideration.

We also find that the generated magnetic field is continuously blown out from the disk on the outflows to the poles, that are driven by the thermal pressure of photoheated gas. The strength of the diffused magnetic field in low density regions is $\sim 10^{-14} - 10^{-13}$ G at $n_{\text{H}} = 10^3 \text{cm}^{-3}$ which could play important roles on the next generation star formation, as well as the seeds of magnetic field exist in present-day universe.

Subject headings: early universe—HII regions — radiative transfer — magnetic fields

1. INTRODUCTION

The energy density of magnetic field in local interstellar gas is not negligible, which plays significant roles on the formation of stars in our Galaxy. This magnetic field is generally regarded as a consequence of dynamo amplification of initial seed magnetic field generated in the early universe. Various generation mechanism of this seed field have been proposed so far: magnetic field generation in the very early universe due to the coupling of gravity and electromagnetic field (e.g. Turner & Widrow 1988), non-zero $\nabla \times \mathbf{E}$ term due to the inhomogeneity of radiation field at the recombination of the universe (e.g. Ichiki et al. 2006), the Biermann battery effect (Biermann 1950) at the shock front in forming galaxies (e.g. Kulsrud et al. 1997; Xu et al. 2008)/ at the ionization fronts in the reionizing universe (Gnedin et al. 2000). It has also been proposed that the radiation force and the Biermann battery effect in the neighbor of luminous sources can generate seed field (Langer et al. 2005; Ando et al. 2010; Doi & Susa 2011). Interestingly, all of these models suggest the seed field strength of $10^{-20} - 10^{-18}$ G at IGM densities, that is well below the observational constraint (Durrer & Neronov 2013, and the references therein).

The generated seed magnetic fields could potentially affect the star formation process in the early universe as seen in our Galaxy, e.g., through launching jets, transferring angular momentum, and suppressing the gravitational fragmentation of disks. It has been pointed out that the resistivity of the primordial gas should be relatively low throughout the collapse of a cloud (e.g. Maki & Susa 2004, 2007; Schleicher et al. 2009). As a result, magnetic fields do not dissipate from the cloud at Jeans scale. Thus, given a same strength of seed magnetic field at the onset of the collapse, magnetic field should have larger impact on star formation in the primordial gas than that in the present-day molecular cloud in which magnetic field dissipate within a certain range of densities (e.g. Nakano & Umebayashi 1986).

Machida et al. (2008) have addressed the dynamical effects of magnetic field on the star formation in primordial gas, assuming ideal MHD, which is correct as far as we consider larger scales than the Jeans length. They found that the magnetic field do have dynamical impact on the collapsing gas including the formation of jets if $B \gtrsim 10^{-9}$ G at 10^3cm^{-3} . Machida & Doi (2013) addressed the later evolution of the system (the gas accretion phase) by resistive MHD calculations. They found that the fragmentation of the disk is significantly suppressed by the magnetic field in case $B \gtrsim 10^{-10} (n_{\text{H}}/10^3 \text{cm}^{-3})^{-2/3}$ G. However if we convert this field strength to the IGM density at $z = 20$ assuming flux freezing, we obtain $B \gtrsim 10^{-14}$ G which is much larger than the seed field strength predicted by various models as mentioned above. Hence, magnetic field seems unlikely to affect the dynamics of the formation of primordial stars. To put it the other way around, if seed field of $B \gtrsim 10^{-14}$ G is generated by some mechanism, magnetic field is a vital part of star formation in the early universe. It has been suggested that small scale turbulence can amplify the seed magnetic field with a dynamical time scale, and it inversely cascade into larger scales to affect the dynamics of star forming cloud at Jeans scale (Schleicher et al. 2010; Schober et al. 2012), although the sufficient amplification to affect the dynamics of the gas has not been shown starting from very weak seed field of $\sim 10^{-18} - 10^{-20}$ G by ab initio

numerical simulations so far (Sur et al. 2010; Federrath et al. 2011; Turk et al. 2012; Latif et al. 2013). In any case the amplitude of seed magnetic field is an important key parameter to understand the primordial star formation.

In this paper, we discuss the seed magnetic field generation mechanism regarding anisotropic radiation field and complex density/temperature structures in the very neighbor of forming first stars, which was originally discussed in our previous studies at 100pc-10kpc scales (Ando et al. 2010; Doi & Susa 2011). We focus on the magnetic field generation especially in the very neighbor of proto-first-stars at 100-1000AU scale where accreting/outflowing gas create intricate structures. Since the generated field strength depends on the radiation flux from the source star, stronger magnetic field is expected.

Such complicated structures have already been calculated by Hosokawa et al. (2011). They investigated the gas accretion process onto a proto-first-star by two dimensional radiation hydrodynamics simulations, although the generation process of magnetic field was not taken into account. In this paper, we evaluate the growth of magnetic field by post-processing scheme utilizing their simulation as a background. Then we discuss the impact of the magnetic field generated through this process on the evolution of the proto-first-stars and the formation of second generation stars.

This paper is organized as follows: we describe the fundamental processes of seed field generation in section 2. In section 3 we show our numerical model, and the results are shown in section 4. Section 5 is devoted to discussion and conclusion.

2. GENERATION OF MAGNETIC FIELD

In this section, we briefly describe the basic equations of magnetic field generation, more detailed description can be found in Ando et al. (2010) though. The growth of magnetic field is described by the following induction equation with two source terms:

$$\frac{\partial \mathbf{B}}{\partial t} = \nabla \times (\mathbf{v} \times \mathbf{B}) - \frac{c}{en_e^2} \nabla n_e \times \nabla p_e - \frac{c}{e} \nabla \times \mathbf{f}_{\text{rad}} \quad (1)$$

This equation is obtained by combining the equation of the force balance on a single electron with the Maxwell's equations. Here we omitted the Hall current term, which is proportional to $\mathbf{j} \times \mathbf{B}$, since this is the higher order term than the others, in case we consider the generation of weak magnetic field.

The first term in the R.H.S. denotes the advection of magnetic field lines which stick to the gas. If the second and third term is neglected, frozen-in condition is satisfied. Thus, the first term is not the source of the magnetic field generation. The second term is the Biermann battery term (Biermann 1950), which is non-zero in case the gradient of electron density and pressure are not perfectly parallel with each other. The third term is the radiation term, which is proportional to the rotation of the radiation force field on a single electron (\mathbf{f}_{rad}).

The radiation force \mathbf{f}_{rad} is composed of two micro processes that could be potentially important for the momentum transfer from photons to electrons. First one is the Thomson scattering. We use formal solution of radiation transfer equation for $\mathbf{f}_{\text{rad,T}}$ as follows:

$$\mathbf{f}_{\text{rad,T}} = \frac{\sigma_{\text{T}}}{c} \int_0^{\nu_L} \mathbf{F}_{0\nu} d\nu + \frac{\sigma_{\text{T}}}{c} \int_{\nu_L}^{\infty} \mathbf{F}_{0\nu} \exp[-\tau_{\nu_L} a(\nu)] d\nu, \quad (2)$$

where $\mathbf{f}_{\text{rad,T}}$ denotes the radiation force per single electron due to Thomson scattering, σ_{T} is the cross section, $\mathbf{F}_{0\nu}$ is the incident energy flux density. ν_L denotes the Lyman-limit frequency, τ_{ν_L} is the optical depth at the Lyman limit regarding the photoionization, and $a(\nu)$ denotes the frequency dependence of photoionization cross section, which is normalized at the Lyman limit, i.e. $a(\nu_L) = 1$ is satisfied.

The second process is the photoionization, whose contribution to \mathbf{f}_{rad} is given as

$$\mathbf{f}_{\text{rad,I}} = \frac{1}{2} \frac{n_{\text{HI}}}{cn_e} \int_{\nu_L}^{\infty} \sigma_{\nu_L} a(\nu) \mathbf{F}_{0\nu} \exp[-\tau_{\nu_L} a(\nu)] d\nu, \quad (3)$$

where σ_{ν_L} denotes the photoionization cross section at the Lyman Limit. We remark that the factor 1/2 in R.H.S. of equation (3) is due to the fact that the photon momentum is equally delivered to protons and electrons. Then, we also can safely assume that only electrons are accelerated by this momentum transfer process, since protons have much larger inertia than electrons.

3. MODEL DESCRIPTION

3.1. The underlying model of proto-first-star formation

We take the underlying model of the proto-first-star formation from Hosokawa et al. (2011). The initial condition of the model is taken from Yoshida et al. (2008), where the formation of the embryo protostar is simulated in a fully cosmological context. The subsequent evolution in the mass accretion stage is followed with 2D radiation hydrodynamic simulations coupled with the protostellar evolution calculations (see Hosokawa et al. 2011 for full details). The stellar mass rapidly increases in this stage, as the gas accretes onto the star through a circumstellar disk. The stellar UV luminosity also sharply rises with increasing the stellar mass, and a bipolar HII region emerges. The HII region then begins to expand dynamically in the accreting envelope, which blows away the gas in the envelope. The circumstellar disk is exposed to the stellar ionizing radiation, and gradually loses its mass owing to the photoevaporation. In the

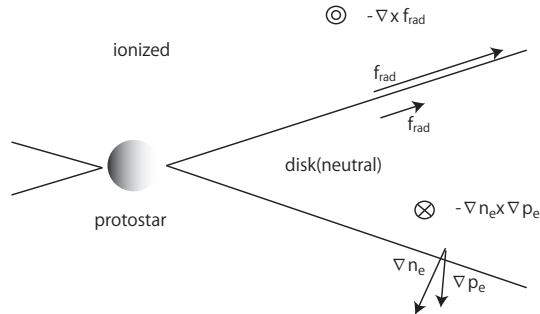


FIG. 1.— Schematic view of magnetic field generation in the neighbor of protostar.

fiducial case, which is adopted here, a $43 M_{\odot}$ star forms as the mass accretion is finally shut off by the stellar UV feedback effect.

3.2. Magnetic field generation by postprocessing

Now we are able to simulate the generation of magnetic field by integrating the equation (1) by postprocessing method utilizing the results of radiation hydrodynamics simulation mentioned above, i.e., the snapshots of the spacial distributions of density, temperature, velocity and chemical abundances in the accretion envelope. Then we assess the Biermann battery term by a simple finite difference scheme. Because of axis symmetry, ∇n_e and ∇p_e are both perpendicular to \mathbf{e}_{ϕ} , the base vector of the azimuthal angle. Thus, the source term $\nabla n_e \times \nabla p_e$ is parallel to \mathbf{e}_{ϕ} (Fig.1).

We can also calculate the radiation term by ray-tracing from the central protostar. This radiation term $\nabla \times \mathbf{f}_{\text{rad}}$ is also directed to \mathbf{e}_{ϕ} , because of the axial symmetry again (Fig.1). We also remark that this term is expected to be significant on the ionization front, where the shear of \mathbf{f}_{rad} is large.

Thus, the seed field generated by these source terms is parallel to \mathbf{e}_{ϕ} . In addition to these source terms, the dynamo term $\nabla \times (\mathbf{v} \times \mathbf{B})$ is also parallel to \mathbf{e}_{ϕ} as long as $\mathbf{B} \propto \mathbf{e}_{\phi}$ is satisfied. Since we assume zero field strength at the initial state in the present simulations, magnetic field is always parallel to \mathbf{e}_{ϕ} throughout the simulation. It is also worth noting that the dynamo term reduces to a simple advection term under the assumed symmetry in the present simulation.

We ignore the contribution from the diffuse radiation emitted from the surface of the disk, since its contribution to the photoionization is smaller than the direct radiation from the protostar.

We use time stepping given by the Courant condition to integrate equation (1), so that we can handle the advection of magnetic field. Since the output interval of the radiation hydrodynamics simulation is larger than the required time step, we interpolate the data between the output time steps.

4. RESULTS

Fig.2 shows the evolution of electron number density and magnetic field around the protostar. Top three panels show the distribution of electron number density on $R - z$ plane of cylindrical coordinate at 1.18×10^4 yrs, 2.02×10^4 yrs, and 7.54×10^4 yrs after the formation of the protostar. Middle panels show the spatial distribution of magnetic field strength at the corresponding epochs. The box is 1800AU on a side. The protostars are located at the bottom left corners of the boxes, and their masses at the three epochs are $17.6 M_{\odot}$, $23.4 M_{\odot}$ and $39 M_{\odot}$, respectively. Bottom row shows the volume weighted probability distribution function on $\log n_{\text{H}} [\text{cm}^{-3}] - \log B [\text{G}]$ plane.

The left column corresponds to the time just after the breakout of ionization front, when the magnetic field is generated in the very neighbor of the protostar. Roughly speaking, the ionized/photoheated small bubble (top) is magnetized (middle). On the other hand, the field strength is weak in the outer less dense regions (bottom).

Another 10^4 yrs later (middle column), an ionization front expand out to this box size to form an hourglass shaped ionized polar region (top). Magnetic field is generated at the ionization front, and the generated magnetic field is transferred to outer less dense regions, riding on the outflow into the polar direction following $B \propto n_{\text{H}}^{2/3}$ law (bottom), roughly.

Finally, at 7.54×10^4 yrs (right column), the generated field strength is $\sim 10^{-14} - 10^{-13} \text{G} (n_{\text{H}}/10^3 \text{cm}^{-3})^{2/3}$ (bottom). This magnitude is still less than the critical field strength shown by white solid line, above which the fragmentation of the accretion disks around proto-first-stars are suppressed (Machida & Doi 2013).

Fig.3 show the Color contour maps of source terms regarding the magnetic field generation at 7.5×10^4 yrs after the formation of the protostar. This epoch corresponds to the final snapshot in Fig.2. Top left panel shows the Biermann battery term, the second term of the left hand side in equation (1), while top right is the radiation term, i.e. the third term in equation (1). The radiation term is prominent at the ionization front, since the shear field of radiation force is maximized at the border between the ionized region and the shadowed neutral region. The Biermann battery term is also important at the ionization front, across which the temperature and the density changes dramatically. We also remark that the Biermann battery term dominates in more extended regions (see bottom left, total source term) since the temperature of the ionized region depends on the distance from the source star very weakly, while the radiation force \mathbf{f}_{rad} is inversely proportional to the square of the distance from the source. Thus, the radiation term dominates

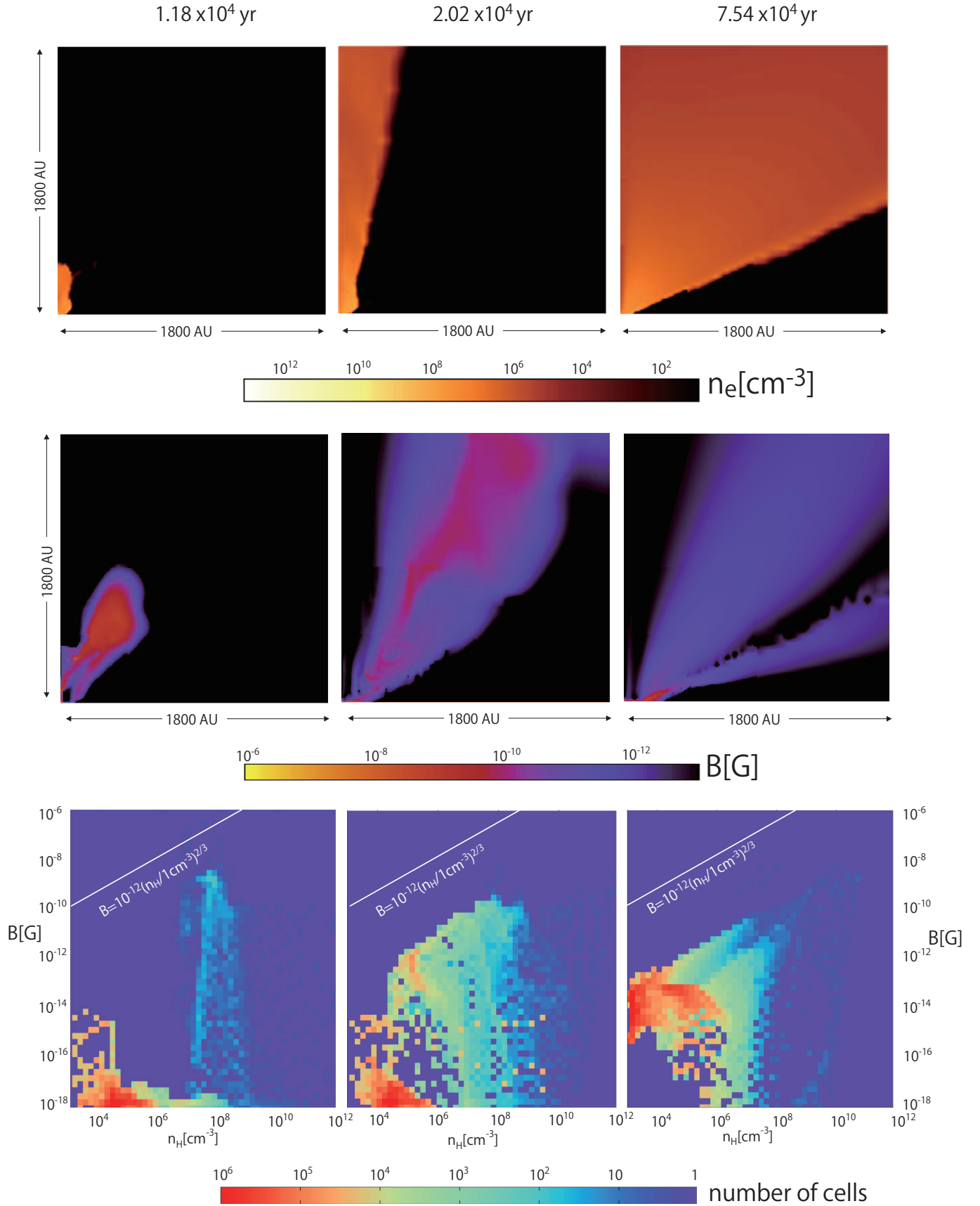


FIG. 2.— Time evolution of magnetic field is presented. Top: electron density n_e is shown by the color contour. In each panel, protostar is located at the left-bottom corner of the box. Three panels corresponds to three snapshots. The box is 1800AU on each side. Three panels correspond to the snapshots of 1.18×10^4 yrs, 2.02×10^4 yrs, and 7.54×10^4 yrs after the formation of the protostar. middle:magnetic field distribution in the neighbor of protostar. Bottom: frequency distribution of computational cells on $\log n_H$ [cm $^{-3}$] – $\log B$ [G] plane.

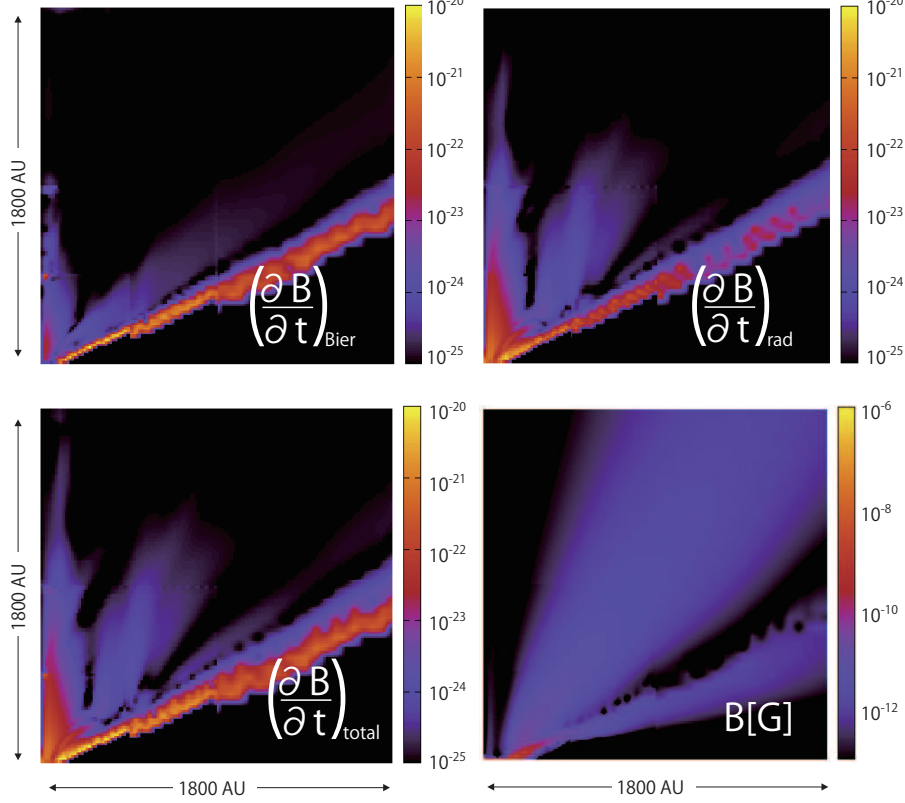


FIG. 3.— Color contour maps of source terms of magnetic field generation. The Biermann battery term (top left), radiation term (top right), total (bottom left), and magnetic field itself (bottom right) at 7.5×10^4 yr after the formation of protostar.

in the neighbor of the protostar. We also mention that the generated magnetic field has smoother structure than the source terms, because the gas temperature/density changes with time and the generated field is transferred to outer less dense regions (bottom right).

Fig. 4 shows the ratio of the radiation term to the Biermann battery term of each cell in the finest numerical box (the nested grid scheme are employed in the RHD simulation). Three colors of points corresponds to the three epochs shown in Fig. 2. It is clear that the Biermann term is more important than the radiation term just after the break out of the ionization front (blue stars), while the radiation term dominates in the later epochs (green and red symbols). This is because the gas is more dynamical in the phase of I-front break out, which leads to larger gradient of density/pressure, so is the Biermann battery term. In the later phase, the density/pressure structure becomes smoother than that in the earlier phase, and the luminosity of ultraviolet radiation from the protostar becomes larger. Thus, the relative importance of radiation source term becomes larger at later epochs.

5. DISCUSSION & CONCLUSION

The magnetic field is generated by two source terms: the radiation term and the Biermann battery term. The order of magnitude of magnetic field strength generated via these processes in the neighbor of the central protostar can be assessed as follows:

$$B_{\text{rad}} \simeq \frac{L \sigma_{\nu_L}}{8 \pi e \Delta r R^2} \Delta t \quad (4)$$

$$B_{\text{Bier}} \simeq \frac{ck_B T \sin \theta}{e \Delta r^2} \Delta t \quad (5)$$

Here, L is the luminosity of the source protostar, Δr denotes the length scale across which f_{rad} or the temperature/density changes, R is the distance from the star, Δt is the duration of field generation, and the θ represents the typical angle between ∇T_e and ∇n_e .

The duration Δt could be assessed as the time scale that the gas is sent brazing out distance R by the outflow of typical velocity v , as $\Delta t \equiv R/v$. Substituting this expression and typical values, we have

$$B_{\text{rad}} \simeq 10^{-9} \text{G} \left(\frac{L}{10^{37} \text{erg/s}} \right) \left(\frac{\Delta r}{10 \text{AU}} \right)^{-1} \left(\frac{R}{100 \text{AU}} \right)^{-1} \left(\frac{v}{30 \text{km/s}} \right)^{-1} \quad (6)$$

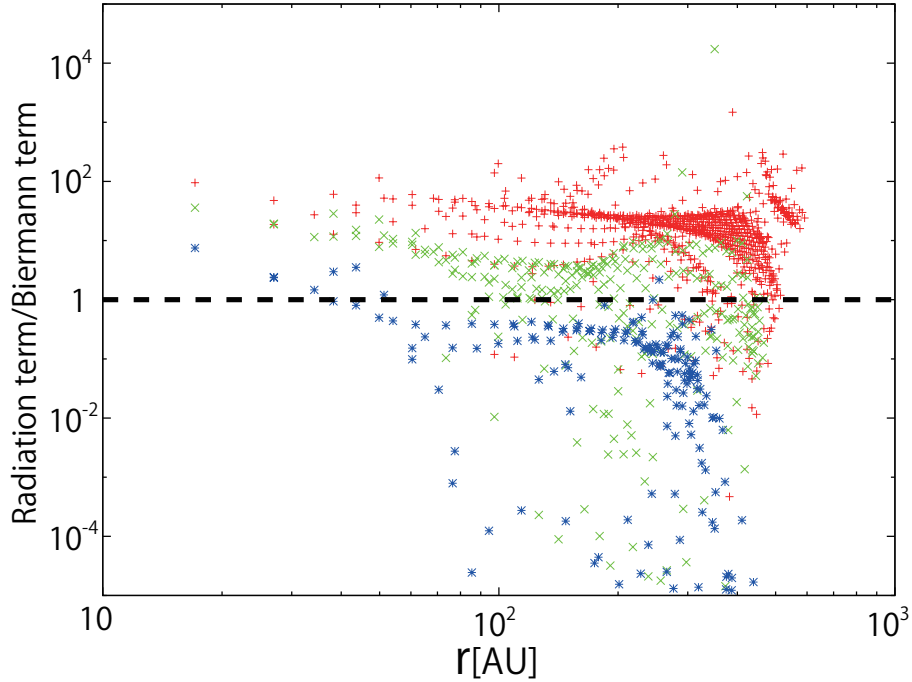


FIG. 4.— The ratio between the radiation source term and the Biermann battery term is plotted as a function of distance from the protostar. Blue stars: 1.18×10^4 yr, Green vertices: 2.02×10^4 yr and Red crosses are for 7.54×10^4 yr. These three snapshots correspond the three panels in Fig. 1. Points above unity (dashed line) denote the grid cell where the radiation term is the dominant source for magnetic field generation.

$$B_{\text{Bier}} \simeq 10^{-12} \text{G} \left(\frac{T_e}{10^4 \text{K}} \right) \left(\frac{\sin \theta}{0.1} \right) \left(\frac{\Delta r}{10 \text{AU}} \right)^{-2} \left(\frac{R}{100 \text{AU}} \right) \left(\frac{v}{30 \text{km/s}} \right)^{-1} \quad (7)$$

Here we assume $\Delta r = 0.1R$. These estimated orders of magnitude are consistent with the numerical results at the inner high density regions, $n_{\text{H}} \gtrsim 10^8 \text{cm}^{-3}$. (see bottom three panels of Fig. 2).

The generate field strength is $\sim 10^{-13} (n_{\text{H}}/10^3 \text{cm}^{-3}) \text{G}$ at the final stage of the present simulation, which is account for $\sim 10^{-17} \text{G}$, at IGM densities of $z = 20$. This magnitude is comparable to the value obtained by previous estimates at 100pc-1kpc scales (Doi & Susa 2011). The coherence length is also similar with each other, since the outflow will extend out to the host minihalos of $\sim 100 \text{pc}$. This obtained field strength is less than the critical value above which the fragmentation of disk is suppressed by two orders of magnitude (Machida & Doi 2013). In addition, we also remark that such relatively large magnetic field emerges after the central protostar grows up to $\gtrsim 20 M_{\odot}$, since the protostar has to be massive enough to emit ultraviolet radiation. According to a three dimensional radiation hydrodynamics simulation, the gas disk is heated by the radiation from the protostar at such epoch, hence the disk is stabilized against gravitational instability (Susa 2013). Thus, the generated magnetic field in this context seems hardly affect the on-site fragmentation of the disk directly.

However, as for the second generation star formation, these field strength could play important roles. Firstly, recent cosmological magneto-hydrodynamics simulations of first star formation revealed that the minihalos that host primordial star forming gas clouds are very turbulent (e.g. Turk et al. 2012). According to the theoretical model, such turbulent motion at much less than the Jeans scale could amplify the seed magnetic field with a dynamical time scale, and it inversely cascade into larger scales to affect the dynamics of star forming cloud at the Jeans scale. If this mechanism also works in the collapsing gas clouds in the neighbor of first stars, the seed field formed in the present mechanism would be important for the formation of second generation stars.

Secondly, we might have underestimated the field strength. According to the equation (6), we have $B_{\text{rad}} \propto R^{-2}$, assuming $\Delta r \simeq 0.1R$. However, the very vicinity around the central protostar is not spatially resolved in the underlying simulations. With the higher-resolution simulations resolving the innermost part of the disk, the magnetic fields generated there should be much stronger than the current estimates. At the disk surface of $R \sim 10 R_{\odot}$, which is slightly larger than the radius of a $40 M_{\odot}$ star, the generated magnetic field could reach $\sim 5 \times 10^{-3} \text{G}$ ¹. We also can assess the density at the surface of the disk of $R \sim 10 R_{\odot}$ by extrapolating the results of numerical simulation, where the gas density is approximately proportional to R^{-1} . Consequently, we obtain $n_{\text{H}} \simeq 2 \times 10^{11} \text{cm}^{-3}$. The generated magnetic field of $\sim 5 \times 10^{-3} \text{G}$ at $n_{\text{H}} \simeq 2 \times 10^{11} \text{cm}^{-3}$ will be blown out to outer less dense regions, and result in $B \sim 10^{-8} \text{G} (n_{\text{H}}/10^3 \text{cm}^{-3})^{2/3}$. This is obviously important for the dynamics of gravitationally collapsing gas cloud even without the amplification by small scale dynamo action quoted in the previous paragraph. However, we remark

¹ It has been pointed out that there is an upper limit of the magnetic field strength generated by radiation drag effects such as the Compton drag (Balbus 1993; Chuzhoy 2004; Silk & Langer 2006). The estimated field strength here is much larger than the limit. However, there is no contradiction because the present radiation effect is not the drag effect.

that higher resolution studies are necessary to find the actual field strength in the very neighbor of the proto-first-star, since this is an estimate based upon the extrapolation of the present results.

We also point out the three dimensional effects can also enhance the magnetic field strength. As shown by recent three dimensional calculations (e.g. Susa 2013), the gas disk around the protostar is highly non-axisymmetric. Such 3D structures induce poloidal component of the magnetic field, which will result in the dynamo amplification in the disk.

In this paper, we assess the magnetic field generated in the very neighbor of proto-first-star due to the Biermann battery effect as well as radiation force. As a result, we find that a weak magnetic field is generated in the inner $\sim 100\text{AU} - 1000\text{AU}$ region and they are blown out to the outer less dense regions riding on the outflows roughly following the $B \propto n_{\text{H}}^{2/3}$ law. The resultant field strength is $B \sim 10^{-14} - 10^{-13}\text{G}(n_{\text{H}}/10^3\text{cm}^{-3})^{2/3}$. This field strength can be the seed magnetic field of the universe and should be important for the next generation star formation, while it hardly affect the dynamics of the on-site first star formation unless very efficient amplification process is taken into consideration.

We thank M. Machida, K. Doi and N. Tominaga for fruitful discussions. This work was supported in part by Ministry of Education, Science, Sports and Culture, Grant-in-Aid for Scientific Research (C), 22540295.

REFERENCES

- Abel T., Norman M. L., Madau P., 1999, *ApJ*, 523, 66
 Abel, T., Bryan, G. L., & Norman, M. L. 2002, *Science*, 295, 93
 Ando, M., Doi, K., & Susa, H. 2010, *ApJ*, 716, 1566
 Balbus, S. A. 1993, *ApJ*, 413, L137
 Biermann, L. 1950, *Zeitschrift Naturforschung Teil A*, 5, 65
 Bisnovatyi-Kogan, G. S., & Blinnikov, S. I. 1977, *A&A*, 59, 111
 Bisnovatyi-Kogan, G. S., Lovelace, R. V. E., & Belinski, V. A. 2002, *ApJ*, 580, 380
 Bisnovatyi-Kogan, G. S., Ruzmaikin, A. A., & Syunyaev, R. A. 1973, *Soviet Astronomy*, 17, 137
 Bromm, V., Coppi, P. S., & Larson, R. B. 2002, *ApJ*, 564, 23
 Chuzhoy, L. 2004, *MNRAS*, 350, 761
 Doi, K., & Susa, H. 2011, *ApJ*, 741, 93
 Durrer, R., & Neronov, A. 2013, *A&A Rev.*, 21, 62
 Federrath, C., Sur, S., Schleicher, D. R. G., Banerjee, R., & Klessen, R. S. 2011, *ApJ*, 731, 62
 Gnedin, N.Y., Ferrara, A., Zweibel, E.G. 2000, *ApJ*, 539, 505
 Harrison, E. R. 1970, *Mon. Not. R.Astron. Soc.* 147, 279
 Hosokawa, T., Omukai, K., Yoshida, N., & Yorke, H. W. 2011, *Science*, 334, 1250
 Ichiki, K., Takahashi, K., Ohno, H., Hanayama, H., Sugiyama, N. 2006, *Sci*, 311, 8271
 Kulsrud, R. M., Cen, R., Ostriker, J. P., & Ryu, D. 1997, *ApJ*, 480, 481
 Lang, K.R.. 1999, *Astrophysical Formulae*(Springer, New York)
 Langer, M., Aghanim, N., & Puget, J.-L. 2005, *A&A*, 443, 367
 Latif, M. A., Schleicher, D. R. G., Schmidt, W., & Niemeyer, J. 2013, *ApJ*, 772, L3
 Machida, M. N., Matsumoto, T., & Inutsuka, S.-i. 2008, *ApJ*, 685, 690
 Machida, M. N., & Doi, K. 2013, *arXiv:1308.2754*
 Maki, H., Susa, H. 2004, *ApJ*, 609, 467
 Maki, H., & Susa, H. 2007, *PASJ*, 59, 787
 Mishustin, I.N., Ruzmaikin, A. A. *Soviet Journal of Experimental and Theoretical Physics*, 1972, 34, 233
 Nakano, T., & Umebayashi, T. 1986, *MNRAS*, 218, 663
 Schneider, R., Ferrara, A., Salvaterra, R., Omukai, K., & Bromm, V. 2003, *Nature*, 422, 869
 Schleicher, D. R. G., Galli, D., Glover, S. C. O., Banerjee, R., Palla, F., Schneider, R., & Klessen, R. S. 2009, *ApJ*, 703, 1096
 Schleicher, D. R. G., Banerjee, R., Sur, S., Arshakian, T. G., Klessen, R. S., Beck, R., & Spaans, M. 2010, *arXiv:1003.1135*
 Schober, J., Schleicher, D., Federrath, C., et al. 2012, *ApJ*, 754, 99
 Shapiro, P.R., Giroux, M.L. 1987, *ApJ*, 321, L107
 Frank, H.Shu. 1992, *GAS DYNAMICS*(University Science Books, California)
 Silk, J., & Langer, M. 2006, *MNRAS*, 371, 444
 Sur, S., Schleicher, D. R. G., Banerjee, R., Federrath, C., & Klessen, R. S. 2010, *ApJ*, 721, L134
 Sur, S., Federrath, C., Schleicher, D. R. G., Banerjee, R., & Klessen, R. S. 2012, *MNRAS*, 423, 3148
 Susa, H. 2013, *ApJ*, 773, 185
 Turk, M. J., Oishi, J. S., Abel, T., & Bryan, G. L. 2012, *ApJ*, 745, 154
 Turner, M.S., Widrow, L.M. 1988, *Phys. Rev.D*, 37, 2743
 Xu, H., O'Shea, B., Collins, D., Norman, M., Li, H., & Li, S. 2008, *ApJ*, 688, L57
 Yoshida, N., Omukai, K., & Hernquist, L. 2008, *Science*, 321, 669